ARTICLE

3D Model Simulating the Hydro-mechanical State of Unsaturated and Deformable Material during Hot air Drying

Lamine Hassini[1,3*]   Sadoth Sandoval Torres[2]

1. University of Tunis El Manar, Faculté des Sciences de Tunis, Laboratoire d'Energétique et des Transferts Thermique et Massique (LETTM), Tunisia
2. Instituto Politécnico Nacional, CIIDIR unidad Oaxaca, Hornos No. 1003, Col. Noche Buena, Santa Cruz Xoxocotlán, Oaxaca, Mexico
3. Department of Physics, College of Science and Humanities in AlGuayah - Shaqra University, Saudi Arabia

ABSTRACT

A three dimensional model to predict the hydro-mechanical state of unsaturated and deformable material during hot air drying has been proposed. The material viscoelastic behaviour was formulated using Bishop's effective stress theory for partially saturated material using the liquid saturation as the Bishop parameter. The hydro-thermal and mechanical equations were coupled by the fluid pressure and the solid matter velocity. The model was applied to a deformable material (innovative clay-cellulose fibers composite) subjected to convective drying. A generalized Maxwell model with five elements, whose parameters were measured experimentally and correlated to water content was used to describe the material's viscoelastic behavior. The hydro-thermal part of the proposed model was validated on the basis of a comparison of experimental and simulated drying rate curves. The Von Mises stress was simulated and compared to the experimental tensile strength in order to predict the time and the region of material failure. For a drying process at 95°C, the region of failure risk was identified. The failure may occur on the lateral surface of the slab in contact with air at a drying time of 2.5h.

1. Introduction

For capillary-porous materials like clay, ceramic and concrete, the most rigorous hydro-mechanical drying models proposed in different previous works assumed that the material was viscoelastic (or plastic) but assumed that the material was saturated throughout drying [1-3]. However, the assumption of a saturated material is a strong hypothesis. Indeed, during the storage, most saturated porous matrices will lose water to the surrounding environment whose relative humidity is less than 100%. This is because an internal gas phase is very likely to appear at the end of the isenthalpic drying period. It seems more appropriate to take into account the existence of the gaseous phase inside the material, since it plays a great role in the development of cracks.

This work aims to present a three dimensional complete drying model to predict the evolution of the hydro-thermal and mechanical state of unsaturated and deformable material during hot air convective drying. The proposed

---

Corresponding Author:
Lamine Hassini,
University of Tunis El Manar, Faculté des Sciences de Tunis, Laboratoire d'Energétique et des Transferts Thermique et Massique (LETTM), Tunisia; Department of Physics, College of Science and Humanities in AlGuayah - Shaqra University, Saudi Arabia; Email: hassini_lamine@yahoo.fr

model is based on our previous publications dealing with mdeling of physical phenomena within porous media during convective and microwave drying [4,5].

The first particularity of our model deals with the mechanical behavoir based on the Bishop's effective stress theory for unsaturated media, where the saturation is the Bishop parameter [6]. The second particularity consists in the testing of a thin slab of clay-cellulosic fiber composite (dimensions: $10\times10\times1cm^3$). This slab constitutes one lateral face of innovative boxes devoted to precious objects and heritage protection against some damages, like fire, moisture, insects, etc. During the drying process, these boxes can undergo some structural mechanical damages and degradations, like cracks, irregular shape, or even fractures when the air drying conditions are not well controlled and scheduled. The hydro-mechanical drying model exposed here can thus be used as a reliable predictive and optimization tool for the industrial drying processes of these composite boxes.

The transport and equilibrium properties required for the implementation of the model were measured and then correlated to temperature and mean moisture content of the studied material. The viscoelastic properties of the material were measured by compressive relaxation testing machine and were then correlated to moisture content. The implementation of the model equations were carried out based on the "COMSOL Multiphysics" solver by using the "PDE coefficient form" mode, the structural mechanics modules and the moving mesh application mode. The hydro-thermal part of the complete model was validated by comparison the experimental and simulated drying rate curves obtained at different drying conditions. The spatio-temporal evolution of the Von Miss stress were simulated and compared to the experimental tensile strength (failure stress) in order to predict the time and the region where the risk of failure can occur. The sample shape was predicted particularly at moment of failure risk.

2. Modeling

2.1 Main Hypothesis of the Model

(1) At the microscopic scale, the studied material is considered multiphase and heterogeneous. However, it is represented by an equivalent homogeneous medium with continuously varying state variables;

(2) The liquid phase is transferred by capillarity due to the water content gradient, by filtration due to the gas phase pressure gradient, and by advection as a result of the hydric shrinkage;

(3) The heat is transferred by conduction and by advection due to the liquid and solid phase flows;

(4) The vapor flows by thermo-diffusion due to temperature gradient, by filtration due to the gas pressure gradient, by diffusion resulting from water content gradient and by advection due to shrinkage;

(5) The shrinkage is isotropic and ideal;

(6) The composite material behaved according to the generalized Maxwell viscoelasticity model consisting of five elements.

2.2 Hydro-thermal Model

The internal hydro-thermal model was based mainly on our previous published work [4]. The full equations' system of the model consists of five partial differential equations: the solid mass balance equation determining the solid (dry matter) concentration (r_s), the dry air transfer equation determining the gas pressure (P_g), the heat transfer equation determining the temperature (T), the liquid water transfer equation determining the liquid water content (X) and the water vapor transfer equation, allowing to calculate the liquid water mass vaporized per unit volume (m_{vap}). The advective terms due to hydric shrinkage are expressed using the solid velocity. This solid velocity was calculated by solving simultaneously the mechanical equation of the hydro-mechanical model.

In order to reduce the length of these equations, the physical parameters representing the material properties were grouped into global coefficients "m"("capacities") and "k"("conductances"). The expressions of these global coefficients are not presented here because of the limited space allocated for this publication.

Solid transfer

$$\frac{\partial \rho_s}{\partial t} = -\text{div}(\rho_s \vec{v}_s) \tag{1}$$

Liquid water transfer

$$m_{22}\frac{\partial X}{\partial t} = div(\alpha_v \vec{v}_s + k_{21}gradT + k_{22}gradX + k_{23}gradP_g) - \rho_s \vec{v}_s gradX \tag{2}$$

$$\alpha_v = \frac{M_v P_v}{RT}\left(\varphi - X\frac{\rho_s}{\rho_l}\right) \tag{3}$$

Heat transfer

$$m_{11}\frac{\partial T}{\partial t} + m_{14}\frac{\partial m_{vap}}{\partial t} = div(k_{11}gradT) - n_l C_{pl}gradT - n_s C_{ps}gradT \tag{4}$$

where n_s and n_l are the solid and the liquid fluxes, re-

spectively given by:

$$n_s = \rho_s \vec{v}_s \tag{5}$$

$$n_l = \rho_s X \vec{v}_s - \frac{K_l^{eq}}{v_l} grad P_g + \frac{K_l^{eq}}{v_l} \frac{\partial P_c}{\partial X} grad X \tag{6}$$

Dry air transfer

$$m_{31}\frac{\partial c_s}{\partial t} + m_{32}\frac{\partial T}{\partial t} + m_{33}\frac{\partial X}{\partial t} + m_{34}\frac{\partial P_g}{\partial t} = div(\alpha_a \vec{v}_s + k_{31} grad T + k_{32} grad X + k_{33} grad P_g) \tag{7}$$

$$\alpha_a = \frac{M_a(P_g - P_v)}{RT}\left(\varphi - X\frac{c_s}{\rho_l}\right) \tag{8}$$

Water vapor transfer

$$m_{44}\frac{\partial m_{vap}}{\partial t} = div(\alpha_v \vec{v}_s + k_{41} grad T + k_{42} grad X + k_{43} grad P_g) \tag{9}$$

The coefficients "m" in the equation (7) depend on dry product porosity f. Due to hydric shrinkage, the material porosity f is not constant but changes continuously during drying. At any instant of drying, the porosity can be calculated by conserving the solid phase mass, which not change during the drying course:

$$\rho_{ss}V(X)(1-\varphi) = \rho_{ss}V_o(1-\varphi_o) \tag{10}$$

where V(X) and V_o are respectively the wet sample volume and the initial sample volume.

2.3 Structural Mechanical Model

The structural mechanical model was based mainly on the mechanical equilibrium equation (Eq. 11), expressed as :

$$\nabla(\sigma_{ij}) = 0 \tag{11}$$

According to Bishop's effective stress concept for partially saturated material [6], the stress tensor s_{ij} can be expressed as [7]:

$$\sigma_{ij} = \sigma_{ij,s} - SP_l - (1-S)P_g \tag{12}$$

where S is the saturation, given by:

$$S = \frac{X}{X_{sat}}; X_{sat} = \varphi\frac{\rho_l}{\rho_s} \tag{13}$$

In the case of viscoelastic behavior, the effective solid stress $s_{ij,s}$ is given by the equation (14), as formulated ed by Rao et al. [8] and used in many previous studies. For our material, the viscoelastic parameters depend both on time and water content:

$$\sigma_{ij,s}(t) = \int_0^t \left(K(t-\tau) - \frac{2}{3}G(t-\tau)\right)\frac{\partial \varepsilon_{kk}(\tau)}{\partial \tau}\delta_{ij}d\tau + 2\int_0^t G(t-\tau)\frac{\partial \varepsilon_{ij}(\tau)}{\partial \tau}d\tau \tag{14}$$

K and G are bulk and shear modulus, respectively. These two parameters were determined on the basis of the following expressions:

$$K(t) = E(t)/2(1+\upsilon) \text{ and } G(t) = E(t)/3(1-2\upsilon) \tag{15}$$

E(t) is the relaxation modulus (the instant elastic modulus) measured experimentally and u is the Poisson's ratio.

According to numerical solution of solid mechanics problems, the above equations are solved in terms of displacements (u) in the three spatial directions. The expressions of the total strain tensor and the solid velocity as a function of displacement according to the small deformation theory are given below:

$$\varepsilon_{ij} = \frac{1}{2}\left(\frac{\partial u_i}{\partial x_j} + \frac{\partial u_j}{\partial x_i}\right); v_s^i = \frac{\partial u_i}{\partial t} \tag{16}$$

2.4 Initial and Boundary Conditions

A. The internal water content, temperature and the gaseous phase pressure were considered initially uniform (atmospheric pressure) and the sample was stress free.

$$X = X_o \; ; \; T = T_o \; ; \; P_o = P_{atm}; \sigma_{ij} = 0 \tag{17}$$

B. At the sample surface in contact with air, the heat and water vapor transfer was assumed to be purely convective and the gas pressure equals to the atmospheric pressure.

$$(n_l + n_v)|_{surf} = k\frac{P_{atm}M_v}{RT_a}\ln\left(\frac{P_{atm} - \phi P_{vsat}(T_a)}{P_{atm} - a_w(X,T)P_{vsat}(T)}\right) \tag{18}$$

$$\lambda_{eq}\frac{\partial T}{\partial n}\bigg|_{surf} + \Delta h_{vap} n_l|_{surf} = h(T_a - T_{surf}) \tag{19}$$

$$P_g^{surf} = P_{atm} \tag{20}$$

C. The local stress normal to the sample surface is zero.

D. The mass and heat transfer and the solid displacement in the y (vertical) direction at the surface in contact with the shelf (y = 0) were negligible.

E. The mass and heat transfer and the solid displacement in the x and z (horizontal) directions at the symmetry planes (x = 0 and z = 0) were nil.

2.5 Model Implementation

For raisons of symmetry (see Figure 1), the constitutive equations of the model were solved on 3D domain, spanning over the quarter of the cellulosic-clay material slab. The model equations as well as the corresponding initial and boundary conditions were numerically implemented in "COMSOL Multiphysics" software, using both the "PDE coefficient form" and the "Structural mechanics" modules and moving mesh application mode. The thermo-physical and viscoelstic properties were experimentally determined and correlated to the state variables X and T, while the hydraulic material properties were adapted from the literature. The convective heat and mass transfer coefficients were estimated using the Chilton-Colburn analogy.
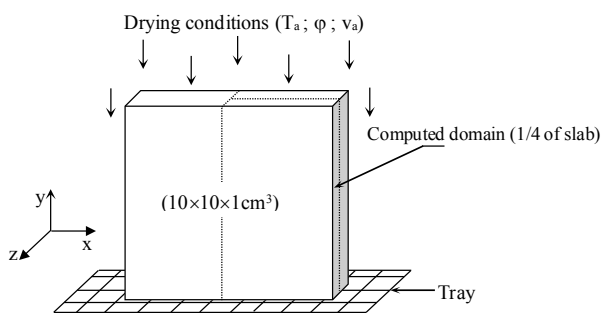

Figure 1. The composite slab orientation in the drying tunnel

3. Simulation Results

3.1 Hydro-thermal State Simulation

The experimental (processed by a moving average filter) and simulated evolution of the drying rate (in terms of water flow rate per unit of sample surface area) versus water content is shown in Figure 2. The drying rate was referred to the current (real) surface area of the slab, which is decreasing during drying as a result of shrinkage. This relevant representation is needed to show the constant rate period which otherwise is merged with the falling rate period. On can observe that the experimental drying curves corresponded well to the simulated ones and the model could then be considered valid. The mean relative error for all drying conditions was less 8%, while a relative error of 10% is generally considered as the worst acceptable value. The deviation between experimental and simulated

curves could be attributed in one part to the mass and surface measurement errors and in the other part to the model hypothesis (mainly that of linear viscoelastic behavior and isotropic hydric shrinkage).
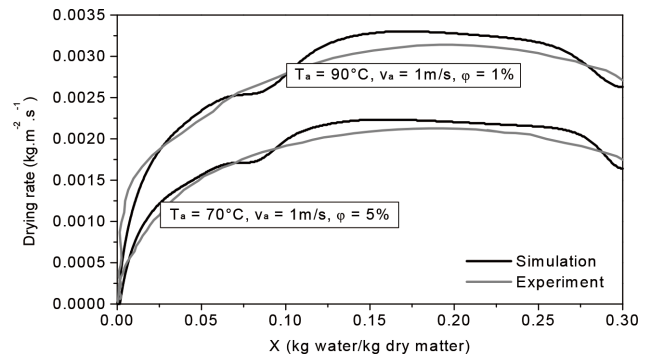

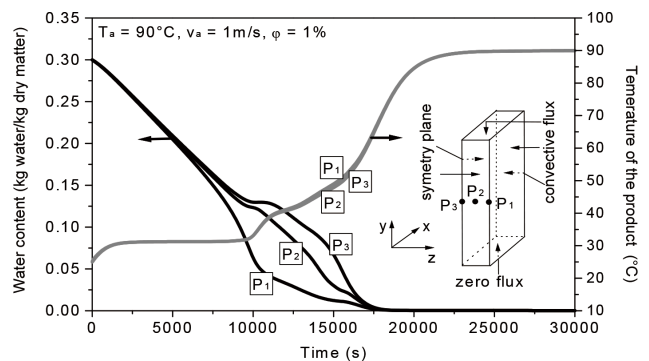**Figure 2.** Drying rate per unit of surface area in function of mean water content

Figure 3. Simulated distributions of temperature and water content

The simulated internal temperature and moisture content distributions within the composite slab (along its thickness in the z direction) are presented in Figure 3. According to these results, one can be observe that the internal temperature profiles exhibited a plateau whose the value corresponding to the wet-bulb temperature of the hot air flow. This fact is confirmed by the constant drying rate phase observed in Figure 2. It can also be seen that, during the falling rate period, the temperature of the sample was nearly uniform. This can be explained by the small thickness of the slab (initially equal to 1cm), and the high thermal conductivity of the moist material (equal to 1.2 W/m/K for moisture content equal to 0.15 kg/kg). Otherwise, the conductivity was around 0.25 W/m/K for moisture content around 0.01kg/kg.

This last result means that the internal water transfer mechanisms (permeation as a result of the internal gaseous phase pressure gradient, capillarity as a result of the liquid water content gradient and advection due to hydric shrinkage) were certainly the limiting phenomena for internal water transfer. This explains the strong moisture content

gradient in the material during this falling rate period. Contrariwise, the moisture content gradient was practically nil during the constant rate period (homogenous drying), in accordance with Salagnac et al. [9] for convective drying of cellular concrete sample. This can be explained by the high water activity due to the high hydraulic material properties (liquid permeability, capillary suction) during this period.

3.2 Mechanical State Simulations

The evolution of normal mechanical stresses (σ_{xx}, σ_{yy} and σ_{zz}) with time, in two specific points of the slab (lateral surface and core of the slab) along the z direction are presented in Figure 4. It can be observed that, the stress changed locally its sign during the drying process. The stress reversal phenomenon is specific to a viscoelastic or plastic behavior as reported in some published reports. It can also be seen that in the three spatial directions, the stress can reached a high levels and thus all normal stresses could contribute to the eventual material damage. In this case (3D geometry), the more relevant criterion to prevent the risks of material damage is the Von Miss stress, which based on an invariant of the stress tensor, and called the "overall" or also the "reduced" stress, in the literature. According to Kowalski [2], this approach is based on the hypothesis of the accumulation of the energy in the stressed material and has the advantage to avoid the analysis of the stresses in each direction. In cartesian coordinates, the Von Mises stress is expressed as:

$$\sigma_{Von\,Mises} = \frac{1}{2}\sqrt{(\sigma_{xx}-\sigma_{zz})^2 + (\sigma_{yy}-\sigma_{zz})^2 + (\sigma_{xx}-\sigma_{yy})^2 + 6\sigma_{xy}^2}$$

(20)

Based on some published works [2,10], the material fracture occurs at a given time and point when the reduced stress exceeds the tensile strength of the dried material. This last should be determined experimentally. In our case, the tensile strength (failure stress) of clay-cellulose fiber composite at dry state was found around 5 MPa.
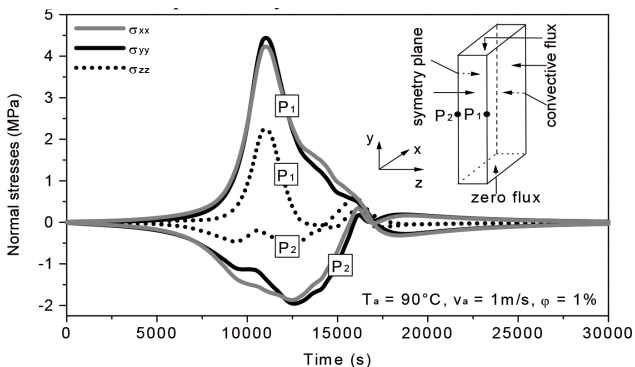

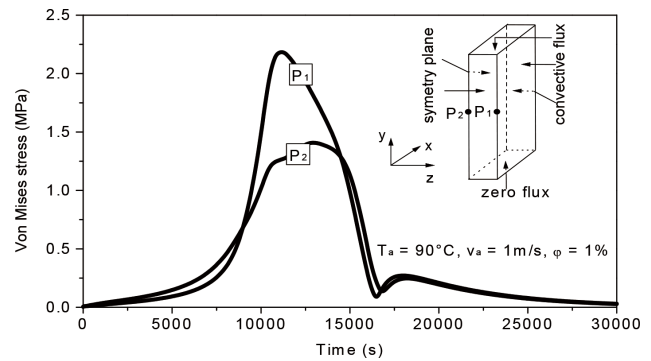**Figure 4.** Normal stress versus time

Figure 5. Von Mises stress versus time

Figure 5 shows the simulated Von Mises stress as a function of time. These profiles are calculated at two specific points of the slab (external surface in contact with air and in the core of the slab) along the z direction. One can observe that the maximum Von Mises stress was located on the sample surface. Based on this result, the risk of cracking affected mainly the external surface of the slab. However, these fissures, if they exist, could not expand into the lower sample part because it was in compression (see Figure 4).

According to Figure 6, for hot air drying process at 95°C, a failure may be occurred on the external surface of the slab after about 2.5h of drying, when the Von Mises stress exceeds the tensile strength. This moment corresponds approximatively to the beginning of the falling rate period (see Figure 3). This cracking time was not far away from the value of 1.85h reported by Kowalski et al. [11] in the case of saturated cylindrical kaolin dried by hot air at 150°C using a linear viscoelastic model. However, it was quite different from 20 h obtained by Musielak [10] for saturated clay plate using an elastic model and a very soft drying condition (air temperature of 60∘C and air relative humidity of 80%). For the drying temperature lower than 95°C, the simulated Von Mises stress value stays well below the tensile strength indicating that there was no material crack (there was not any failure observed on the upper surface of the sample at drying temperature 90°C). Figure 6 shows also the simulated slab shape at moment of failure (the external frame represents the initial sample contour while the internal one corresponds to the real sample contour). One can note that during the drying process, the sample decreases in volume but retains its rectangular shape. This could be explained by the highly elastic character of this material during the falling rate period.
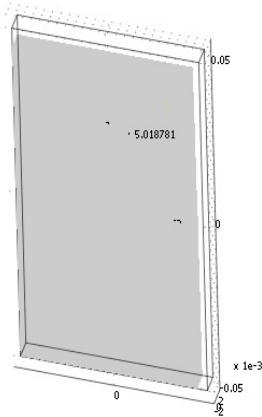
Figure 6. Region of the material's fracture

4. Conclusion

An internal comprehensive drying model simulating the hydro-thermo-viscoelastic state of an unsaturated and deformable material has been developed. This complete model coupling all transfer mechanisms (advection, capillarity, filtration, ,…) and structural mechanics. Its particularity lies in the structural mechanical part which is based on the Bishop's effective stress equation using the liquid saturation as the Bishop parameter. The mechanical part and the hydro-thermal par of the complete model were coupled by the fluid pressure and the solid matter velocity. The "COMSOL Multiphysics" software was used to numerically implemented the model equations. The model was aplied to an innovative material based on clay-cellulosic fibers subjected to hot air drying. The prediction of the cracking risk was realized on the basis of the comparison of the Von Mises stress and the experimental tensile stress. For a drying process at 95°C, the region of failure risk was localized. The failure may occur on the lateral surface of the slab in contact with air at a drying time of 2.5h. For lower drying temperature, the simulation indicated that there was no material fracture, in accordance with the experimental observations. The hydro-thermo-viscoselastic model developed here can thus be used as a reliable predictive and optimization tool for industrial drying processes involving innovative ceramic materials undergoing substantial shrinkage and intense water vaporization.

References

[1] S.J. Kowalski, J. Banaszak, A. Rybicki. Plasticity in materials exposed to drying, Chem Eng Sci. 2010, 65: 5105-5116.

[2] S.J. Kowalski. Control of mechanical processes in drying. Theory and experiment, Chem Eng Sc. 2010, 65: 890-899.

[3] J. Banaszak, S.J. Kowalski. Theoretical and experimental analysis of stresses and fractures in clay like materials during drying, Chem. Eng. and Process. 2005, 44: 497-503.

[4] L. Hassini, R. Peczalski, J.-L. Gelet. Drying of granular medium by hot air and microwaves. Modeling and prediction of internal gas pressure and binder distribution, Powder Technol. 2015a, 286: 636-644.

[5] L. Hassini, L., Peczalski, R., Laurent, P., Azzouz, S.. 2-D hydro-viscoelastic model for convective drying of highly deformable water saturated product, Dry. Technol., 2015b, 33: 1872-1882

[6] Bishop, A.W.. The principle of effective stress, Tek. Ukebl., 1959, 39: 859-863

[7] W.G. Gray, B.A.. Schrefler. Analysis of the solid phase stress tensor in multiphase porous media, Int. J. Numer. Anal. Methods Geomech. 2007, 31(4): 541-581

[8] V.N.M. Rao, D.D. Hamann, J.R. Hammerle. Stress analysis of a viscoelastic sphere subjected to temperature and moisture gradients, J. Agr. Eng. Res. 1975, 20(3): 283–293.

[9] P. Salagnac, P. Glouannec, D. Lecharpentier. Numerical modeling of heat and mass transfer in porous medium during combined hot air, infrared and microwaves drying, Int. J. Heat Mass Transf. 2004, 47: 4479-4489

[10] G. Musielak. Possibility of clay damage during drying, Dry. Technol. 2001, 19(8): 1645-1659

[11] S.J. Kowalski, K. Rajewska, A. Rybicki. Stresses generated during convective and microwave drying, Dry. Technol. 2005, 2: 1875-1893